Available online at www.sciencedirect.com
SCIENCE DIRECT®
ELSEVIER
International Journal of Solids and Structures 42 (2005) 951–970
INTERNATIONAL JOURNAL OF SOLIDS and STRUCTURES
www.elsevier.com/locate/ijsolstr

Role of elasticity in elastic–plastic fracture. Analytical bi-linear crack-tip fields and finite element analysis

Changlu Tian [a,*], Yunxin Gao [b]

[a] China Ship Scientific Research Center, P.O. Box 116, Wuxi, Jiangsu 214082, China
[b] Department of Materials, Imperial College London, Exhibition Road, London SW7 2AZ, UK

Received 5 May 2004
Available online 18 August 2004

Abstract

A solution for Model-I plane strain crack tip fields in a bi-linear elastic–plastic material is presented. The elastic–plastic Poisson's ratio is introduced to characterize the influence of elastic deformation on the near tip constraint. Attention is focused on the distribution of elastic/plastic strain energy in the sensitive region of the forward sector ahead of a crack tip. The present study shows that the elastic strain energy can be higher than the plastic strain energy in this sensitive sector while large amount of the plastic strain energy develops outside this sector around the crack tip. The effect of elastic deformation in this sensitive region on the structure of crack-tip fields is considerable and the assumption in some important solutions for crack-tip fields reported in literature that the elastic deformation is small and can be ignored is therefore not physically reasonable. Besides, finite element analysis is carried out to validate the analytical solution and good agreement between them is found. It is seen that the present solution with T-stress can properly describe the crack-tip fields under various constraints for different specimens and an analytical relation is established between the critical value of J-integral, J_c, and T-stress for elastic–plastic fracture.

Keywords: Crack-tip field; Elastic–plastic fracture; Elastic effect

1. Introduction

Solutions for crack-tip fields are important in understanding the mechanisms of crack initiation and propagation in elastic–plastic materials. It is a milestone in the development of elastic–plastic fracture mechanics that the well-known HRR singularity (Hutchinson, 1968a; Rice and Rosengren, 1968) was published and the J-integral fracture criterion was established based on this solution. However, some limitations or flaws were found in the HRR solution and J-integral criteria. Many works based on finite element method (FEM) demonstrated that the crack-tip fields for different specimen geometries are not in line with HRR solution (McMeeking, 1977; McMeeking and Parks, 1979; Shih and German, 1981;

* Corresponding author. Tel.: +86-0510-5556214; fax: +86-0510-5556897.
E-mail addresses: cltian197@imut.edu.cn, cltian@cssrc.com.cn (C. Tian).

0020-7683/$ - see front matter © 2004 Elsevier Ltd. All rights reserved.
doi:10.1016/j.ijsolstr.2004.05.015

Hutchinson, 1983; Shih, 1985, etc.). Meanwhile, some experimental results showed that the critical value of J-integral, which was deemed to be a material constant, is dependent on the specimen geometry (Begly and Lands, 1972; Hancock and Cowling, 1980). Therefore, many studies were contributed to modify the HRR solution to achieve physically reasonable fracture criteria.

There is a general agreement that the effect of elasticity on elastic–plastic crack-tip fields is relatively small as compared with that of plasticity and therefore can be omitted. However, many studies showed that this elastic effect cannot be simply ignored and more studies are needed. These important results on this topic are subsequently reviewed in details to address the role of elastic strain energy. The constitutive equation of plastic deformation theory is

$$\frac{\varepsilon_{ij}}{\varepsilon_0} = (1+\nu)\frac{S_{ij}}{\sigma_0} + \frac{1-2\nu}{3}\frac{\sigma_{kk}}{\sigma_0}\delta_{ij} + \frac{3}{2}\alpha\left(\frac{\sigma_e}{\sigma_0}\right)^{n-1}\frac{S_{ij}}{\sigma_0}. \tag{1}$$

In Eq. (1), the strain components ε_{ij} are related to the deviation stress components S_{ij} of stress tensor σ_{ij}, $S_{ij} = \sigma_{ij} - \sigma_m\delta_{ij}$. The mean stress is expressed as $\sigma_m = (\sigma_r + \sigma_\theta + \sigma_z)/3$ with out-plane stress component σ_z and in-plane stresses σ_r, σ_θ under plane strain condition (see Fig. 1). As usual, E and ν are the Young's modulus and Poisson's ratio, and σ_0 denotes the initial yield stress and $\varepsilon_0 = \sigma_0/E$ is the corresponding strain, respectively. The stress components are related to a stress function $\phi(r,\theta)$ in the form of

$$\sigma_r = r^{-1}\phi' + r^{-2}\ddot{\phi}, \quad \sigma_\theta = \phi'', \quad \sigma_{r\theta} = -(r^{-1}\dot{\phi})', \tag{2}$$

where $()'$ and $\dot{()}$ denote the derivatives of $\phi(r,\theta)$ with respect to the near tip coordinates r, θ respectively, see Fig. 1.

In addition, the compatibility equation is

$$r^{-1}(r\varepsilon_\theta)'' + r^{-1}\varepsilon_r - r^{-1}\ddot{\varepsilon}_r - 2r^{-2}(\varepsilon_{r\theta})' = 0. \tag{3}$$

Generally, the stress function is assumed in a separable form and the higher order asymptotic form of $\phi(r,\theta)$ is in the form of

$$\phi(r,\theta) = K_1 r^{s_1+2}\tilde{\phi}_1(\theta) + K_2 r^{s_2+2}\tilde{\phi}_2(\theta) + \cdots \tag{4}$$

with K_1, K_2, S_1, and S_2 as unknown constants to be determined by boundary conditions. With the help of Eqs. (1)–(4), the higher-order-term solutions were obtained (Li and Wang, 1986; Xia et al., 1993), but the effective stress σ_e in their solutions was in the form of

$$\sigma_e = \left[(3/4)\cdot(\sigma_r - \sigma_\theta)^2 + 3\sigma_{r\theta}^2\right]^{\frac{1}{2}}. \tag{5}$$

However, the definition of effective stress σ_e is,

$$\sigma_e = (1/\sqrt{2})\cdot\left[(\sigma_r - \sigma_\theta)^2 + (\sigma_\theta - \sigma_z)^2 + (\sigma_z - \sigma_r)^2 + 6\sigma_{r\theta}^2\right]^{\frac{1}{2}}. \tag{6}$$

It is noted that Eq. (5) is derived from Eq. (6) under the full plastic assumption of $\sigma_z = 0.5(\sigma_r + \sigma_\theta)$. For plane strain problems ($\varepsilon_z = 0$), Eq. (1) gives

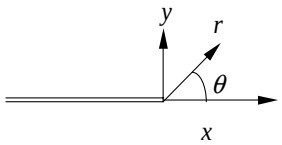

Fig. 1. Crack-tip coordinate system.

$$\sigma_z/(\sigma_r+\sigma_\theta)=v_{\mathrm{ep}}=f(v,E,\alpha,\sigma_0,\sigma_{\mathrm{e}}/\sigma_0). \tag{7}$$

Eq. (7) describes the dependence between σ_z and σ_{e}, and gives the definition of v_{ep}, which is referred as the elastic–plastic Poisson's ratio in this paper. From Eqs. (6) and (7), it is seen that σ_z and σ_{e} are dependent on each other. Because of this dependence, σ_{e} cannot be independently expressed by the in-plan stress components, and thus solving the crack-tip asymptotic fields cannot be carried on. This problem was fixed by assuming v_{ep} to be 0.5 (Li and Wang, 1986; Xia et al., 1993). However, the assumption of $\sigma_z=0.5(\sigma_r+\sigma_\theta)$ holds true only when the ratio of plastic to elastic deformation is infinite, i.e. $\varepsilon_{\mathrm{p}}/\varepsilon_{\mathrm{e}}\to\infty$, and in real elastic–plastic problems, the value of $\sigma_z/(\sigma_r+\sigma_\theta)$ changes from v to 0.5 (Guo, 1993). The change of v_{ep} has a considerable effect on the stress/stain fields in the sensitive region ahead of a crack tip. Therefore, further studies on this subject are expected.

Many multi-term solutions were studied (O'Dowd and Shih, 1991a,b; Sharma and Aravas, 1991; Xia et al., 1993; Yang et al., 1993, etc.). Some of these studies reported that only the third or higher order terms of the solutions were affected by elastic deformation and therefore the effect of elasticity could be omitted. For example, in the solution presented by Sharma and Aravas (1991), the strain function was expressed as

$$\varepsilon(r,\theta)/\alpha\varepsilon_0=r^{sn}\varepsilon^{(0)}(\theta)+r^{s(n-1)+t}\varepsilon^{(1)}(\theta)+r^{s}\varepsilon^{e(0)}(\theta)+\cdots, \tag{8}$$

where s, t is the power of stress function and $s>t$; n is the hardening exponent. The first two terms represents the plastic strain where $s=-1/(n+1)$ and $t<(n-2)/(n+1)$. The third term represents the elastic strain. Therefore, it was concluded that the effects of elasticity enter the solution in the higher order terms of the asymptotic solutions. However, the above result was derived by comparing only the powers of the radial coordinate r without considering the angular coordinate θ. The typical angular distribution of the plastic strains $\tilde{\varepsilon}^{\mathrm{p}}(\theta)$ around a crack reported by Hutchinson (1968b) showed that $\varepsilon^{\mathrm{p}}(\theta)$ approaches zero as $\theta\to 0^\circ$. The fact is that r^{sn}, $r^{s(n-1)+t}>r^s$ as $r\to 0$, but both $\varepsilon^{(0)}(\theta)$ and $\varepsilon^{(1)}(\theta)$ of Eq. (8) approach zero while $\varepsilon^{e(0)}(\theta)$ approach a finite value as $\theta\to 0^\circ$ (see Tian and Wen, 2001). Therefore, it cannot be concluded that the third elastic term is always less than the first two plastic terms on the ligament. In other words, whether the first two plastic terms are the dominant ones depends on the other coordinate θ. This problem is also related to the assumption of the separable stress function of the common asymptotic analysis. Yang et al. (1993) also obtained multi-term solutions. In the common asymptotic analysis for a series expansion of r, as r approaches zero, the coefficients of each term of different order of r was taken to be zero. The equation of $\tilde{\sigma}_{zz}^{(1)}=\tilde{\sigma}_{\mathrm{m}}^{(1)}=0.5(\tilde{\sigma}_r^{(1)}+\tilde{\sigma}_\theta^{(1)})$ of the first term was obtained for plane strain problems ($\varepsilon_z=0$). This equation is just the incompressible one and so the first term is still the HRR singularity. The incompressible or full plastic result is related to the assumption that stress function is separable in r and θ, which is a far more complicated problem and needs further study.

Sharma and Aravas (1991) also remarked that the dominant region of the two-term stress ahead of the crack is smaller than that in the angular region $60^\circ<\theta<180^\circ$, which raises the question as to whether the two-term expansion can provide an accurate description of the stress field in the region ahead of a crack. Therefore, it is expected to get the more reasonable crack tip fields in the region $0^\circ<\theta<60^\circ$ where the fracture process takes place.

An alternative approach of solving the crack-tip fields in a bi-linear elastic–plastic material was presented by Yang and Chao (1992) as well as Chao and Yang (1992) in which the constitutive relation was

$$\varepsilon_{ij}=\frac{1+v}{E}S_{ij}+\frac{1-2v}{3E}\sigma_{kk}\delta_{ij}+\frac{3}{2}\left(\frac{1}{E_{\mathrm{p}}}-\frac{1}{E}\right)(1-\bar{\sigma}_{\mathrm{e}}^{-1})S_{ij}. \tag{9}$$

They still employed the assumption of $\bar{\sigma}_{\mathrm{e}}=\sigma_{\mathrm{e}}/\sigma_0\to\infty$ and so the factor of $(1-\bar{\sigma}_{\mathrm{e}}^{-1})$ in Eq. (9) vanished. This implies that the ratio of plastic to elastic deformation is infinite, i.e. $\varepsilon_{\mathrm{p}}/\varepsilon_{\mathrm{e}}\to\infty$. The present study shows that the values of the normalized equivalent stress $\sigma_{\mathrm{e}}/\sigma_0$ ahead of a crack tip are not very large and

the near-tip field is very sensitive to the values of σ_e/σ_0. Therefore, the assumption of $\bar{\sigma}_e = \sigma_e/\sigma_0 \to \infty$ is not reasonable.

The full plastic models are consciously or unconsciously employed in the analysis of elastic–plastic fracture as reviewed above. However, the negligence of the above-mentioned elastic effect can be one of the considerable reasons responsible for the invalidation of the J-integral based criterion. Little studies of elastic effects on elastic–plastic fracture processes have been reported although many multi-term solutions were obtained. The current study presents an alternative attempt to consider the elastic effect. Some merits of the elastic–plastic Poisson's ratio v_{ep} are discussed for plane-strain problems. The patterns of near-tip energy distributions under different constraints are presented. The present study provides a new insight into the role of elasticity in elastic–plastic fracture.

2. An analogy solution for elastic–plastic near-tip fields

2.1. The analogy between elastic–plastic and linear elastic problems

To investigate elastic–plastic near-tip fields, an analogy analysis is presented in this section. For the sake of usefulness, the basic equations of linear elastic crack-tip field are transcribed here. The sum of the first two terms of the right-hand side of Eq. (1) or Eq. (9) is elastic stress–strain relation is

$$\varepsilon_{ij} = \frac{1+v}{E} S_{ij} + \frac{1-2v}{3E}\sigma_{kk}\delta_{ij}. \tag{10}$$

The compatibility equation is Eq. (3) and the linear crack-tip field was obtained by Williams (1957). The integral J is related to the stress intensity factor K_I as $J = (1-v^2)K_I^2/E$ since $\varepsilon_z = 0$, $\sigma_z = v(\sigma_r + \sigma_\theta)$ for mode-I plane strain crack. The linear elastic crack-tip stress field can be written in form of

$$\begin{bmatrix} \sigma_r & \sigma_{r\theta} \\ \sigma_{\theta r} & \sigma_\theta \end{bmatrix} = \left[\frac{EJ}{2\pi(1-v^2)r}\right]^{\frac{1}{2}} \begin{bmatrix} \tilde{\sigma}_r & \tilde{\sigma}_{r\theta} \\ \tilde{\sigma}_{\theta r} & \tilde{\sigma}_\theta \end{bmatrix} + \begin{bmatrix} \cos^2\theta & -\sin\theta\cos\theta \\ -\sin\theta\cos\theta & \sin^2\theta \end{bmatrix} T. \tag{11a}$$

The second term of the right-hand side of Eq. (11a) denotes the so-called T-stress. It has a finite or bounded value and can be regarded as the stress acting parallel to the crack flanks (Rice, 1974). In addition, the θ-variations were

$$\begin{cases} \tilde{\sigma}_r(\theta) = \dfrac{1}{4}\left(5\cos\dfrac{\theta}{2} - \cos\dfrac{3}{2}\theta\right), \\ \tilde{\sigma}_\theta(\theta) = \dfrac{1}{4}\left(3\cos\dfrac{\theta}{2} + \cos\dfrac{3}{2}\theta\right), \\ \tilde{\sigma}_{r\theta}(\theta) = \dfrac{1}{4}\left(\sin\dfrac{\theta}{2} + \sin\dfrac{3}{2}\theta\right). \end{cases} \tag{11b}$$

To demonstrate the analogy method, the bi-linear elastic–plastic model is studied. Fig. 2 shows the uniaxial stress–strain relation where E_p is the tangent modulus of elastic–plastic stress–strain curve (i.e., the less

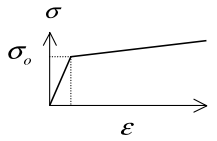

Fig. 2. Elastic–plastic stress–strain relation.

steep line as $\sigma > \sigma_0$) and σ_0 is the initial yield stress. In the multi-axial stress state, it is in the form of Eq. (9) and can be rewritten as

$$\varepsilon_{ij} = \frac{1+v+\lambda}{E} S_{ij} + \frac{1-2v}{3E}\sigma_{kk}\delta_{ij} \tag{12a}$$

with

$$\lambda = \frac{3}{2}\left(\frac{E}{E_p} - 1\right)(1 - \bar{\sigma}_e^{-1}). \tag{12b}$$

By introducing two elastic–plastic parameters v_{ep}, E_{ep} defined as

$$\frac{1+v_{ep}}{E_{ep}} = \frac{1+v+\lambda}{E}, \quad \frac{1-2v_{ep}}{3E_{ep}} = \frac{1-2v}{3E}, \tag{13}$$

we rearrange Eq. (12a) as

$$\varepsilon_{ij} = \frac{1+v_{ep}}{E_{ep}} S_{ij} + \frac{1-2v_{ep}}{3E_{ep}}\sigma_{kk}\delta_{ij}. \tag{14}$$

It is clearly seen that the form of Eq. (14) is the same as that of Eq. (10), but the two elastic constants E and v in Eq. (10) are replaced by the two elastic–plastic variables E_{ep} and v_{ep} in Eq. (14). These two parameters are defined by Eq. (13) and they are the requirements of the analogy between the elastic model and elastic–plastic model. On the basis of Eqs. (12b) and (13), we obtain the following expressions,

$$E_{ep} = \frac{E}{1+2\lambda/3} = \frac{E}{1+(n_p-1)(1-\bar{\sigma}_e^{-1})}, \tag{15}$$

$$v_{ep} = \frac{v+\lambda/3}{1+2\lambda/3} = \frac{v+(n_p-1)(1-\bar{\sigma}_e^{-1})/2}{1+(n_p-1)(1-\bar{\sigma}_e^{-1})} \tag{16}$$

with $n_p = E/E_p$ for short. In addition, the following equations are hold,

$$\left.\begin{array}{l} \lambda = 3(v_{ep}-v)/(1-2v_{ep}) \\ E_{ep} = E\cdot(1-2v_{ep})/(1-2v) \end{array}\right\}. \tag{17}$$

Because of the important role in elastic–plastic crack-tip fields to be demonstrated in the following sections, v_{ep} is known as elastic–plastic Poisson's ratio.

2.2. The role of v_{ep} in elastic–plastic plane strain problems

Under the plane strain condition ($\varepsilon_z = 0$), Eq. (14) leads to

$$v_{ep} = \sigma_z/(\sigma_r + \sigma_\theta). \tag{18}$$

Obviously, v_{ep} coincides with the constraint parameter $\sigma_z/(\sigma_r+\sigma_\theta)$ under the plane strain condition. It is noted that v_{ep} was introduced and defined by Eq. (13). From Eq. (16), we obtain

$$v_{ep} = v, \quad \text{as } \bar{\sigma}_e = \sigma_e/\sigma_0 = 1.0, \tag{19a}$$

$$v_{ep} \to v_{max} = \frac{1}{n_p}\left[v + \frac{1}{2}(n_p-1)\right], \quad \text{as } \bar{\sigma}_e = \sigma_e/\sigma_0 \to \infty. \tag{19b}$$

Therefore, v_{ep} is in the range of $v \leqslant v_{ep} < v_{max}$. It is clear that v_{ep} depends not only on materials constants v and n_p, but also on the normalized effective stress $\bar{\sigma}_e = \sigma_e/\sigma_0$, which is a measure of the degree of plastic deformation level.

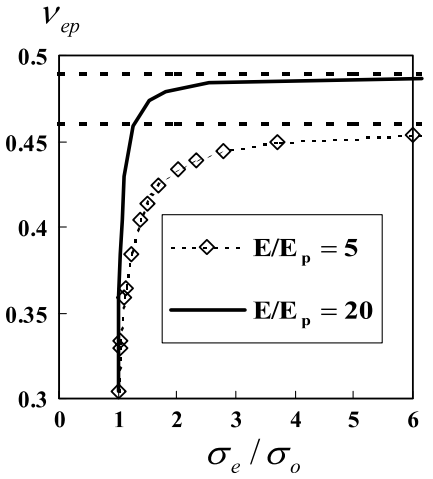

Fig. 3. The elastic–plastic Poisson's ratio to effective stress for plane strain problems.

Fig. 3 shows the dependence of v_{ep} on σ_e/σ_0 as expressed by Eq. (16) for the cases of $v = 0.3$, $n_p = E/E_p = 5$, 20 where the dash lines denote the values of v_{max}. It can be seen that the assumption of $v_{ep} = 0.5$ means both σ_e/σ_0 and E/E_p approach to infinite. It will be seen in the following sections that the change of v_{ep} or $\bar{\sigma}_e = \sigma_e/\sigma_0$ induces a great change of the near-tip fields, especially the near-tip energy distribution.

2.3. Solution procedure of elastic–plastic crack tip fields

On the basis of the analogy between Eqs. (10) and (14), replacing v and E in Eq. (11a) with v_{ep} and E_{ep} gives

$$\begin{bmatrix} \sigma_r & \sigma_{r\theta} \\ \sigma_{\theta r} & \sigma_\theta \end{bmatrix} = \left[\frac{E_{ep}J}{2\pi(1-v_{ep}^2)r}\right]^{\frac{1}{2}} \begin{bmatrix} \tilde{\sigma}_r & \tilde{\sigma}_{r\theta} \\ \tilde{\sigma}_{\theta r} & \tilde{\sigma}_\theta \end{bmatrix} + \begin{bmatrix} \cos^2\theta & -\sin\theta\cos\theta \\ -\sin\theta\cos\theta & \sin^2\theta \end{bmatrix} T. \tag{20a}$$

With the help of Eq. (17) and $\sigma_0 = \sqrt{E\sigma_0\varepsilon_0}$, Eq. (20a) can be written as

$$\begin{bmatrix} \sigma_r & \sigma_{r\theta} \\ \sigma_{\theta r} & \sigma_\theta \end{bmatrix} \Big/ \sigma_0 = \left[\frac{(1-2v_{ep})}{2\pi(1-v_{ep}^2)(1-2v)\varepsilon_0}\left(\frac{1}{r\sigma_0/J}\right)\right]^{\frac{1}{2}} \begin{bmatrix} \tilde{\sigma}_r & \tilde{\sigma}_{r\theta} \\ \tilde{\sigma}_{\theta r} & \tilde{\sigma}_\theta \end{bmatrix} + \begin{bmatrix} \cos^2\theta & -\sin\theta\cos\theta \\ -\sin\theta\cos\theta & \sin^2\theta \end{bmatrix} \frac{T}{\sigma_0}. \tag{20b}$$

Apparently, the elastic–plastic crack-tip field was analogically obtained. Unfortunately, Eq. (20b) is not the final elastic–plastic solution, because v_{ep} and E_{ep} are not material constants but dependent on the stress components in elastic–plastic cases. This implies that the compatibility equation cannot be exactly satisfied. However, Eq. (20b) provides an effective way to solve the elastic–plastic fields. Although v_{ep} changes from one point to another in the elastic–plastic fields, it has a certain value at a given point with the dimensionless coordinate $(r\sigma_0/J, \theta)$. For a given point $(r\sigma_0/J, \theta)$, the value of v_{ep} at this point can be determined by an iteration procedure. By substituting Eq. (20b) into the expression (6) of the effective stress σ_e, we obtain a $v_{ep} \sim \sigma_e$ relation at the given point. Bearing in mind, we already have another $v_{ep} \sim \sigma_e$ relation of Eq. (16) illustrated in Fig. 3 and it can be rewritten as

$$\frac{\sigma_e(n_p, v_{ep})}{\sigma_0} = \frac{(n_p - 1)(0.5 - v_{ep})}{(n_p - 1)(0.5 - v_{ep}) + v - v_{ep}}. \tag{21}$$

The combination of these two $v_{ep} \sim \sigma_e$ relations determines the value of v_{ep} at the given point. In other words, the two relations can be illustrated as two curves, and the value of v_{ep} at the intersecting point of these two curves is the real value of v_{ep} at the given point $(r\sigma_0/J, \theta)$. As the above-mentioned procedure is carried out repeatedly from one point to another, the values of v_{ep} are determined at all points around the crack-tip. With the determined value of v_{ep} at a given point, the stress components at the given point are given by Eq. (20b). Consequently, the elastic–plastic solutions for crack-tip fields are obtained. Some solutions for specific cases of consideration are discussed in the following sections.

3. Stress and strain crack-tip fields

3.1. Stress and strain distributions under high constraint of $T/\sigma_0 = 0$

When $\overline{T} = T/\sigma_0 = 0$, the second term of Eq. (20b) vanishes, and the effective stress is obtained by substituting Eq. (18), and the first term (the so-called high constraint crack tip field) of Eq. (20b) into (6), namely,

$$\frac{\sigma_e(r\sigma_0/J, \theta, v_{ep})}{\sigma_0} = \left[\frac{(1 - 2v_{ep})}{2\pi(1 - v_{ep}^2)(1 - 2v)\varepsilon_0} \cdot \left(\frac{1}{r\sigma_0/J}\right)\right]^{\frac{1}{2}} \left[(1 - 2v_{ep})^2 + 3\sin^2\frac{\theta}{2}\right]^{\frac{1}{2}} \cos\frac{\theta}{2}. \tag{22}$$

By using the above-mentioned procedure, the value of v_{ep} can be determined by Eqs. (21) and (22). The values of v_{ep} at some points of interest are determined, including points at $r\sigma_0/J = 2, 5$ and $\theta = 0°, 10°, \ldots, 180°$ (angular distribution) as well as points at $\theta = 0°$, $r\sigma_0/J = 1.0, 1.5, \ldots, 6.0$ (ligament distribution, see Section 3.2). The results for two different materials ($v = 0.3$, $\varepsilon_0 = 0.002$, $n_p = E/E_p = 5, 20$) are showed in Fig. 4.

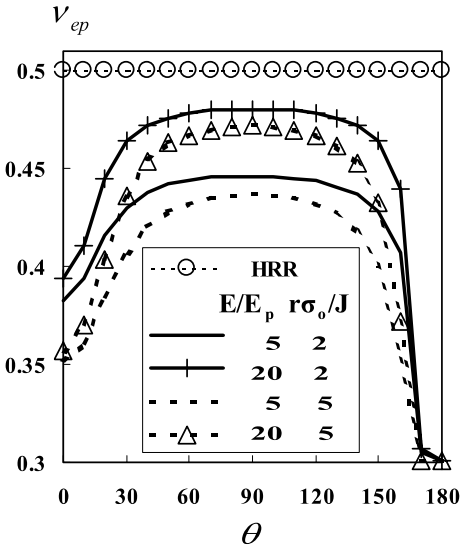

Fig. 4. Angular distribution of elastic–plastic Poisson's ratio for $T/\sigma_0 = 0$, $E/E_p = 5, 20$.

It is found that the value of v_{ep} in the forward sector ($|\theta| < 30°$, $1 < r\sigma_0/J < 5$) is obviously smaller than 0.5, it is noted that $\sigma_z/(\sigma_r + \sigma_\theta) = 0.5$ in the HRR solution.

The stress components at each point $(r\sigma_0/J, \theta)$ can be obtained by substituting v_{ep} at the point into Eq. (20b) with $\overline{T} = T/\sigma_0 = 0$. With the help of Eqs. (9), (12) and (17), the elastic and plastic strain components are expressed as

$$\varepsilon_{ij}^{e} = \frac{1+v}{E} S_{ij} + \frac{1-2v}{3E}\sigma_{kk}\delta_{ij}, \tag{23a}$$

$$\varepsilon_{ij}^{p} = \frac{\lambda}{E} S_{ij} = \frac{3(v_{ep}-v)}{1-2v_{ep}} \frac{S_{ij}}{E}. \tag{23b}$$

With Eq. (18) and $\sigma_{kk} = 3\sigma_m = (1+v_{ep})(\sigma_r + \sigma_\theta)$, substituting Eq. (20b) with $\overline{T} = T/\sigma_0 = 0$ into Eqs. (23a) and (23b) leads to

$$\bar{\varepsilon}_{ij} = \frac{\varepsilon_{ij}}{\varepsilon_0} = \left[\frac{(1-2v_{ep})}{2\pi(1-v_{ep}^2)(1-2v)\varepsilon_0} \cdot \left(\frac{1}{r\sigma_0/J}\right)\right]^{\frac{1}{2}} \tilde{\varepsilon}_{ij}(\theta) \tag{24a}$$

with the functions of $\tilde{\varepsilon}_{ij}(\theta)$ for total strain, and $\tilde{\varepsilon}_{ij}^{e}(\theta)$, $\tilde{\varepsilon}_{ij}^{p}(\theta)$ for elastic, plastic strain,

$$\begin{cases} \tilde{\varepsilon}_r^{e}(\theta) = \dfrac{1+v}{4}\left(5\cos\dfrac{\theta}{2} - \cos\dfrac{3}{2}\theta\right) - 2v(1+v_{ep})\cos\dfrac{\theta}{2}, \\ \tilde{\varepsilon}_\theta^{e}(\theta) = \dfrac{1+v}{4}\left(3\cos\dfrac{\theta}{2} + \cos\dfrac{3}{2}\theta\right) - 2v(1+v_{ep})\cos\dfrac{\theta}{2}, \\ \tilde{\varepsilon}_{r\theta}^{e}(\theta) = \dfrac{1+v}{4}\left(\sin\dfrac{\theta}{2} + \sin\dfrac{3}{2}\theta\right). \end{cases} \tag{24b}$$

and

$$\begin{cases} \tilde{\varepsilon}_r^{p}(\theta) = \dfrac{3(v_{ep}-v)}{1-2v_{ep}}\left[\dfrac{1}{4}\left(5\cos\dfrac{\theta}{2} - \cos\dfrac{3}{2}\theta\right) - \dfrac{2}{3}(1+v_{ep})\cos\dfrac{\theta}{2}\right], \\ \tilde{\varepsilon}_\theta^{p}(\theta) = \dfrac{3(v_{ep}-v)}{1-2v_{ep}}\left[\dfrac{1}{4}\left(3\cos\dfrac{\theta}{2} + \cos\dfrac{3}{2}\theta\right) - \dfrac{2}{3}(1+v_{ep})\cos\dfrac{\theta}{2}\right], \\ \tilde{\varepsilon}_{r\theta}^{p}(\theta) = \dfrac{3(v_{ep}-v)}{(1-2v_{ep})} \cdot \dfrac{1}{4} \cdot \left(\sin\dfrac{\theta}{2} + \sin\dfrac{3}{2}\theta\right). \end{cases} \tag{24c}$$

The strain components for two different materials ($v = 0.3$, $\varepsilon_0 = 0.002$, $E/E_p = 5$, 20) are determined. The angular distribution of elastic strain ε_{ij}^{e} and total strain ε_{ij} at $r\sigma_0/J = 2$ are showed in Fig. 5. It is clearly seen that the elastic strain is nearly the dominant term in the forward sector ($|\theta| < 30°$). It is noted that the strains on the ligament in the HRR solution are zero (see Hutchinson, 1968b).

3.2. Elastic–plastic Poisson's ratio for various T-stress values

The distribution of the elastic–plastic Poisson's ratio on the ligament for various values of T-stress (different constrains) is of interest in this section. On the ligament ($\theta = 0°$), Eq. (20b) leads to

$$\begin{bmatrix} \sigma_r & \sigma_{r\theta} \\ \sigma_{\theta r} & \sigma_\theta \end{bmatrix} \Big/ \sigma_0 = \left[\frac{(1-2v_{ep})}{2\pi(1-v_{ep}^2)(1-2v)\varepsilon_0} \cdot \left(\frac{1}{r\sigma_0/J}\right)\right]^{\frac{1}{2}} \begin{bmatrix} 1 & 0 \\ 0 & 1 \end{bmatrix} + \begin{bmatrix} \overline{T} & 0 \\ 0 & 0 \end{bmatrix}. \tag{25}$$

Under the plane strain condition, with Eq. (18), substituting (25) into (6) gives

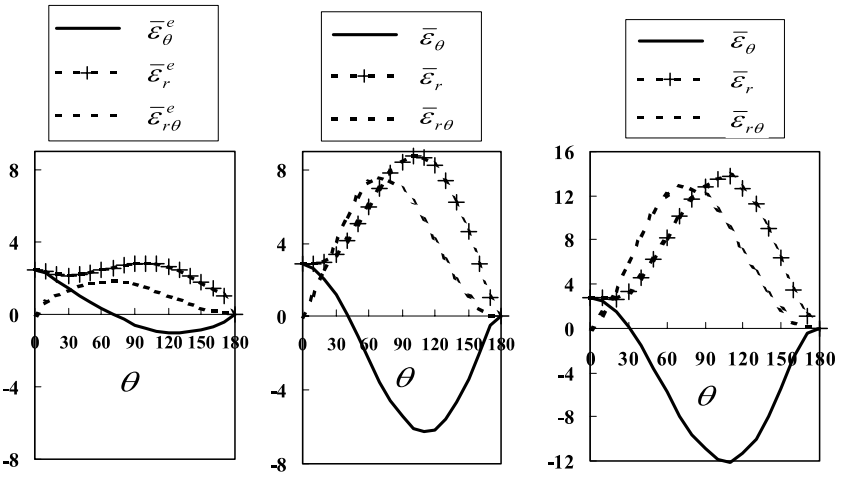

(a) Elastic strain for $E/E_P = 5$ (b) Total strain for $E/E_P = 5$ (c) Total strain for $E/E_P = 20$

Fig. 5. Angular distributions of elastic, plastic and total strains for $T/\sigma_0 = 0$.

$$\bar{\sigma}_e = \sigma_e/\sigma_0 = \left[(1 - v_{ep} + v_{ep}^2)\overline{T}^2 + (1 - 2v_{ep})^2\overline{T}\bar{\sigma}_\theta + (1 - 2v_{ep})^2\bar{\sigma}_\theta^2\right]^{\frac{1}{2}} \tag{26a}$$

with $\bar{\sigma}_\theta$ as

$$\bar{\sigma}_\theta = \left[\frac{(1 - 2v_{ep})}{2\pi(1 - v_{ep}^2)(1 - 2v)\varepsilon_0} \cdot \left(\frac{1}{r\sigma_0/J}\right)\right]^{\frac{1}{2}}. \tag{26b}$$

Similarly, Eqs. (21) and (26) leads to

$$\left[(1 - v_{ep} + v_{ep}^2)\overline{T}^2 + (1 - 2v_{ep})^2\overline{T}\bar{\sigma}_\theta + (1 - 2v_{ep})^2\bar{\sigma}_\theta^2\right]^{\frac{1}{2}} = \frac{(n_p - 1)(0.5 - v_{ep})}{(n_p - 1)(0.5 - v_{ep}) + v - v_{ep}}. \tag{27a}$$

Substituting (26b) into (27a) gives the dependence of v_{ep} on $\overline{T} = T/\sigma_0$. It can be expressed as

$$v_{ep} = v_{ep}(T/\sigma_0, r\sigma_0/J, v, \varepsilon_0, n_p). \tag{27b}$$

For example, two hardening materials with $v = 0.3$, $n_p = E/E_p = 5$, $\varepsilon_0 = \sigma_0/E = 0.002$, and $v = 0.3$, $n_p = E/E_p = 20$, $\varepsilon_0 = \sigma_0/E = 0.0028$ are discussed. The later is similar to HY80 steel ($n = 9$ for power hardening material, $E = 200$ MPa, $\sigma_0 = 560$ MPa, $v = 0.3$, from Hancock and Cowling, 1980). Based on these material data, the relation $v_{ep} = v_{ep}(T/\sigma_0, r\sigma_0/J, v, \varepsilon_0, n_p)$ is obtained by using Eqs. (27a) and (26b). The ligament distributions of v_{ep} for different values of T-stress are plotted in Fig. 6.

It is clearly seen that the all values of v_{ep} are lower than 0.5 and increase as the "constraint" decreases. In addition, it is noted that the value of σ_m/σ_e depends on the value of v_{ep}, and it is generally overestimated by assuming $v_{ep} = 0.5$. As a constraint parameter, v_{ep} is directly in the expressions of the crack tip field in bi-linear materials, and can directly represent the ratio of elastic to plastic deformation.

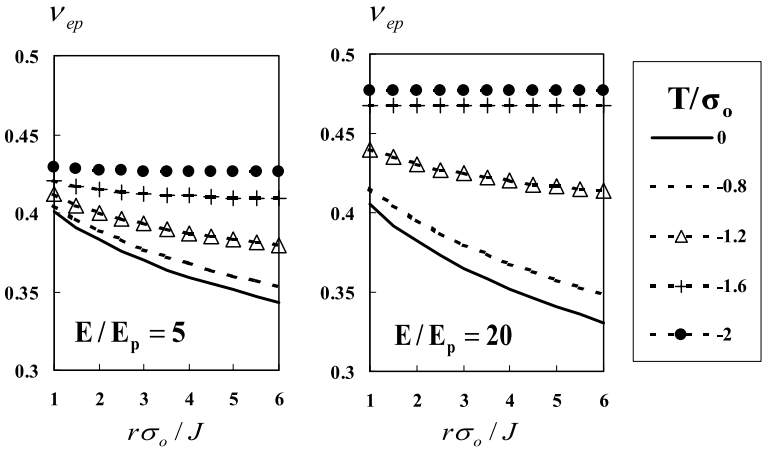

Fig. 6. Ligament distribution of elastic–plastic Poisson's ratio of different T-stress values for $E/E_{\mathrm{p}} = 5$, 20.

4. Crack-tip energy fields in bi-linear materials

4.1. The energy distributions for high constraints of $T/\sigma_0 = 0$

Since the elastic–plastic strain energy fields is significantly important in terms of the construction of a physically reasonable failure criterion, we discuss the case under high constraint ($\overline{T} = T/\sigma_0 = 0$) in this section. With the elastic, plastic strain $\varepsilon_{ij}^{\mathrm{e}}$, $\varepsilon_{ij}^{\mathrm{p}}$ of Eq. (23a) and (23b), the densities of elastic and plastic strain energy can be deduced by the definition

$$w_{\mathrm{e}} = \int \sigma_{ij} d\varepsilon_{ij}^{\mathrm{e}} = \frac{1+v}{3E}\sigma_{\mathrm{e}}^2 + \frac{3(1-2v)}{2E}\sigma_{\mathrm{m}}^2, \tag{28a}$$

$$w_{\mathrm{p}} = \int \sigma_{ij} d\varepsilon_{ij}^{\mathrm{p}} = \frac{\lambda}{3E}\sigma_{\mathrm{e}}^2 = \frac{v_{\mathrm{ep}} - v}{1-2v_{\mathrm{ep}}}\frac{\sigma_{\mathrm{e}}^2}{E}. \tag{28b}$$

The stresses of singularity term (or the high constraint fields) are determined by (20b) with $\overline{T} = T/\sigma_0 = 0$. With the help of Eq. (18), by substituting the stresses into (28), we obtain the energy densities as

$$\left[\frac{w_{\mathrm{e}}}{\sigma_0\varepsilon_0}, \frac{w_{\mathrm{p}}}{\sigma_0\varepsilon_0}\right] = \frac{(1-2v_{\mathrm{ep}})J}{2\pi(1-v_{\mathrm{ep}}^2)(1-2v)\sigma_0\varepsilon_0 r}[\tilde{w}_{\mathrm{e}}(\theta), \tilde{w}_{\mathrm{p}}(\theta)], \tag{29a}$$

where the functions of $\tilde{w}_{\mathrm{e}}(\theta), \tilde{w}_{\mathrm{p}}(\theta)$ are in the form of

$$\begin{cases} \tilde{w}_{\mathrm{e}}(\theta) = \dfrac{1}{3}\left[(1+v)(1-2v_{\mathrm{ep}})^2 + 2\cdot(1-2v)(1+v_{\mathrm{ep}})^2 + 3(1+v)\sin^2\dfrac{\theta}{2}\right]\cos^2\dfrac{\theta}{2}, \\ \tilde{w}_{\mathrm{p}}(\theta) = \dfrac{v_{\mathrm{ep}} - v}{1-2v_{\mathrm{ep}}}\left[(1-2v_{\mathrm{ep}})^2 + 3\sin^2\dfrac{\theta}{2}\right]\cos^2\dfrac{\theta}{2}. \end{cases} \tag{29b}$$

The angular distributions ($r\sigma_0/J = 2$) of the ratio of elastic to total strain energy density $w_{\mathrm{e}}/(w_{\mathrm{e}} + w_{\mathrm{p}})$ for two materials given in Section 3.2 are presented in Fig. 7. It is clearly showed that the elastic strain energy is the dominant term and therefore the omission of elasticity is not physically applicable in the forward sector ($\theta < 30°$).

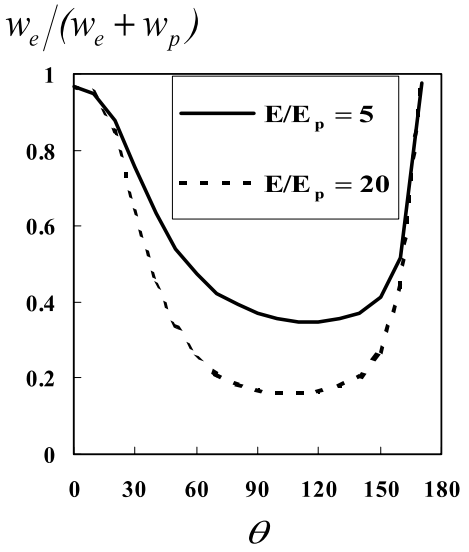

Fig. 7. Angular distribution of the ratio of elastic to total strain energy density for $T/\sigma_0 = 0$, $E/E_p = 5$, 20.

4.2. Elastic and plastic energy distributions for various T-stress values

The ligament ($\theta = 0$) field for various values of T/σ_0 (the different constrains) is the topic of this section. The energy density can also be deduced by the definition. The combination of Eqs. (18), (25), (26), (28a) and (28b) leads to the expressions of the elastic energy density w_e and plastic energy density w_p, and they are written in the following dimensionless form,

$$\bar{w}_e = \frac{1+v}{3}\cdot\left[(1-v_{ep}+v_{ep}^2)\overline{T}^2 + (1-2v_{ep})^2\overline{T}\bar{\sigma}_\theta + (1-2v_{ep})^2\bar{\sigma}_\theta^2\right] + \frac{3(1-2v)}{2}\cdot\left[\frac{1}{3}\cdot(1+v_{ep})\cdot(2\bar{\sigma}_\theta+\overline{T})\right]^2, \tag{30a}$$

$$\bar{w}_p = \frac{v_{ep}-v}{1-2v_{ep}}\cdot\left[(1-v_{ep}+v_{ep}^2)\overline{T}^2 + (1-2v_{ep})^2\overline{T}\bar{\sigma}_\theta + (1-2v_{ep})^2\bar{\sigma}_\theta^2\right]. \tag{30b}$$

By substituting v_{ep} (Fig. 6 or Eq. (27)) into Eqs. (30a) and (30b), the energy distributions can be calculated. The ligament distributions of the elastic and plastic strain energy densities of various values of T/σ_0 for $E/E_p = 5$, 20 are plotted in Figs. 8 and 9. It is seen that w_p values of $E/E_p = 5$ keeps very low, while the w_p curves of $E/E_p = 20$ increase sharply after T/σ_0 reaches value about $T/\sigma_0 = -1.0$, which is accompanied with decreasing of elastic energy density w_e. Again, it is not acceptable ignoring the elastic effects on the ligament. Together with Fig. 7, it is clearly shows that the elastic strain energy is the dominant term in the forward sector ($|\theta| < 30°$) in the annulus of $1 < r\sigma_0/J < 6$ around a crack tip while the plastic strain energy is dominant term in the area out of the forward sector.

4.3. Total energy distributions for various T-stress values

The distribution of total strain energy density on the ligament is useful in aiding the understanding of fracture processes. The sum of Eqs. (30a) and (30b) gives the dimensionless form of total strain energy density, and it can be simplified as

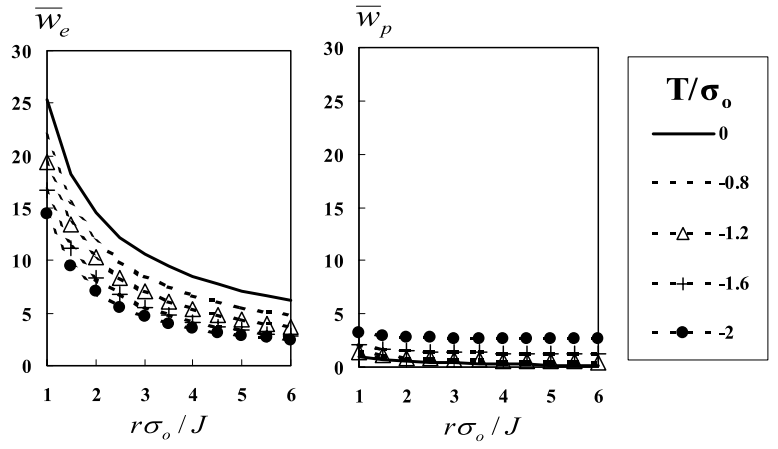

Fig. 8. Ligament distribution of elastic, plastic energy density of different T-stress values for $E/E_{\mathrm{p}} = 5$.

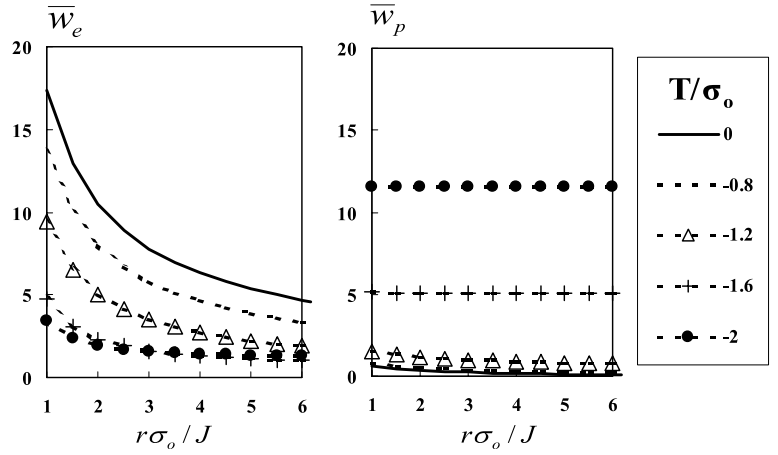

Fig. 9. Ligament distribution of elastic, plastic energy density of different T-stress values for $E/E_{\mathrm{p}} = 20$.

$$\bar{w}_{\mathrm{ep}} = (\bar{w}_{\mathrm{ep}})_{\mathrm{I}} + (\bar{w}_{\mathrm{ep}})_{\mathrm{II}} \tag{31a}$$

with $(\bar{w}_{\mathrm{ep}})_{\mathrm{I}}$ and $(\bar{w}_{\mathrm{ep}})_{\mathrm{II}}$ as

$$(\bar{w}_{\mathrm{ep}})_{\mathrm{I}} = \frac{(1-2\nu_{\mathrm{ep}})J}{2\pi(1-\nu_{ep})\sigma_0\varepsilon_0 r}, \tag{31b}$$

$$(\bar{w}_{\mathrm{ep}})_{\mathrm{II}} = \left[\frac{(1+\nu_{\mathrm{ep}})(1-2\nu)(1-2\nu_{\mathrm{ep}})J}{2\pi(1-\nu_{\mathrm{ep}})\sigma_0\varepsilon_0 r}\right]^{\frac{1}{2}}\overline{T} + \frac{(1-2\nu)(1-\nu_{\mathrm{ep}}^2)}{2(1-2\nu_{\mathrm{ep}})}\overline{T}^2. \tag{31c}$$

Substituting $\nu_{\mathrm{ep}} = \nu_{\mathrm{ep}}(T/\sigma_0, r\sigma_0/J, \nu, \varepsilon_0, n_{\mathrm{p}})$ for $E/E_{\mathrm{p}} = 20$ (Fig. 6) into (31b) and (31c) gives the distribution of $(\bar{w}_{\mathrm{ep}})_{\mathrm{I}}$, $(\bar{w}_{\mathrm{ep}})_{\mathrm{II}}$ as shown in Fig. 10 where the energy terms are plotted again the positions on ligament under various constraints.

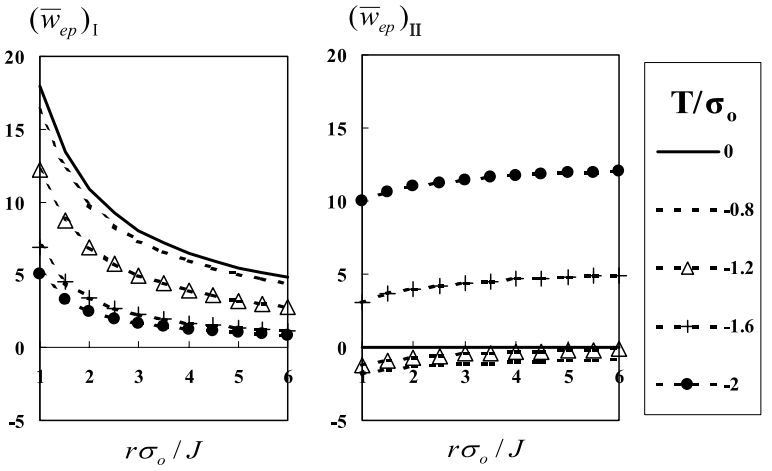

Fig. 10. Ligament distribution of total energy density of different T-stress values for $E/E_{\mathrm{p}} = 20$.

It is found that $(\bar{w}_{\mathrm{ep}})_{\mathrm{I}}$ decreases but $(\bar{w}_{\mathrm{ep}})_{\mathrm{II}}$ increases as the T/σ_0 decrease. In addition, $(\bar{w}_{\mathrm{ep}})_{\mathrm{II}}$ keeps a very low value until T/σ_0 reach a certain value (about $T/\sigma_0 = -1.0$), then it increases sharply when $T/\sigma_0 < -1.0$. It should be noted that $(\bar{w}_{\mathrm{ep}})_{\mathrm{II}}$ can becomes negative as $T/\sigma_0 > -1.0$, but the total energy is always positive. It is also seen that a factor of $1/(1-2\nu_{\mathrm{ep}})$ is included in Eqs. (31c) and (30b). Therefore, $(\bar{w}_{\mathrm{ep}})_{\mathrm{II}}$ and w_{p} increase rapidly as $\nu_{\mathrm{ep}} \to 0.5$. This phenomenon can also be found from Fig. 6 compared with Figs. 9 and 10.

5. Finite element analysis

For the validation and application of the bi-linear crack-tip fields presented above, this section examines the same crack-tip fields by using finite element method (FEM). Analyses on the elastic–plastic energy distributions around a crack are addressed again numerically. And the materials data used here are the same as the analytical analysis above.

As shown in Fig. 11, two kinds of typical specimens, three-point bend bar (TPB) and centre-cracked panel (CCP) are studied. The ratio of the crack length over the specimen width, a/W, is taken as $a/W = 0.5$ in the above-mentioned two cases.

Fig. 12 illustrates the finite element meshes, where the region near the crack-tip is modelled with refined meshes, and the radial length of the element close to crack tip is 0.001 of the ligament size. In this FEM analysis, ANSYS Version 5.6.2 (ANSYS 5.6.2, 2000) is employed, the element type is chosen as eight-node iso-parameter element. About 500 increments are applied to cover the range from small-scale yielding to the deep yielding.

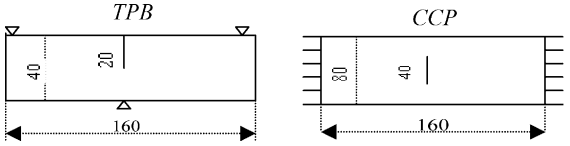

Fig. 11. Two typical specimens for FEM analyses.

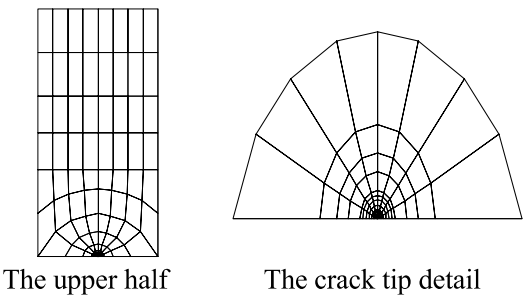

Fig. 12. Finite element mesh.

5.1. Distributions of elastic–plastic Poisson's ratio v_{ep} around crack tip

The angular distributions at $r\sigma_0/J = 2$ of v_{ep} of high constraint specimen (TPB) for $E/E_p = 5$, 20 and the ligament distributions of v_{ep} of the two typical specimens (TPB and CCP) for $E/E_p = 20$ are presented in Fig. 13.

From the analytical results of Figs. 4 and 6 as well as the FEM results of Fig. 13, it is showed that the curves of FEM results of TPB are similar to those of the bi-linear field of $T = 0$. From high to low constraints, the FEM results of two typical specimens are similar to those given by the bi-linear field from high T-stress values to low. Both of them shows that v_{ep} is considerably lower than 0.5 in the forward sector $|\theta| < 30°$.

Figs. 4, 6 and 13 also show that the v_{ep} values change from 0.35 to 0.48 in the range of $1 < r\sigma_0/J < 6$ on the ligament. The values of σ_e/σ_0 in this range is not very large (generally less than 3.0, see Fig. 3), and v_{ep} is very sensitive to σ_e/σ_0 in this range as showed in Fig. 3. Therefore, both assumptions of $\bar{\sigma}_e = \sigma_e/\sigma_0 \to \infty$ and $\sigma_z/(\sigma_r + \sigma_\theta) = 0.5$ employed in literature reviewed previously are not applicable.

5.2. Energy distribution around crack tip

The angular distributions ($r\sigma_0/J = 2$) of the ratio of elastic to total energy density obtained by FEM analyses of $E/E_p = 5$, 20 for high constraint specimen (TPB) are illustrated in Fig. 14. The ligament

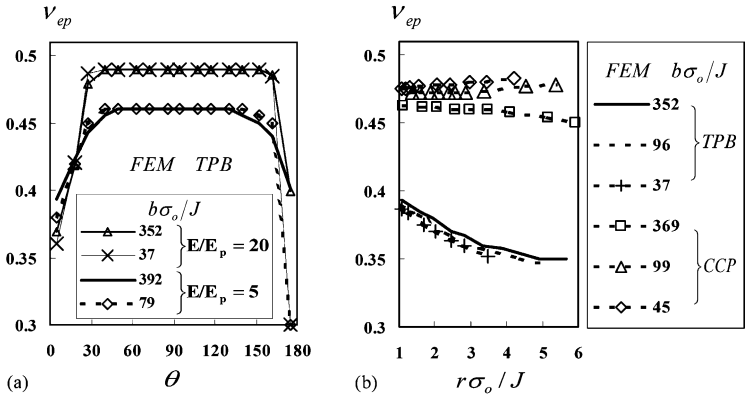

Fig. 13. Distribution of elastic–plastic Poisson's ratio around a crack tip. (a) Angular distribution for $E/E_p = 5$, 20 and (a) ligament distribution for $E/E_p = 20$.

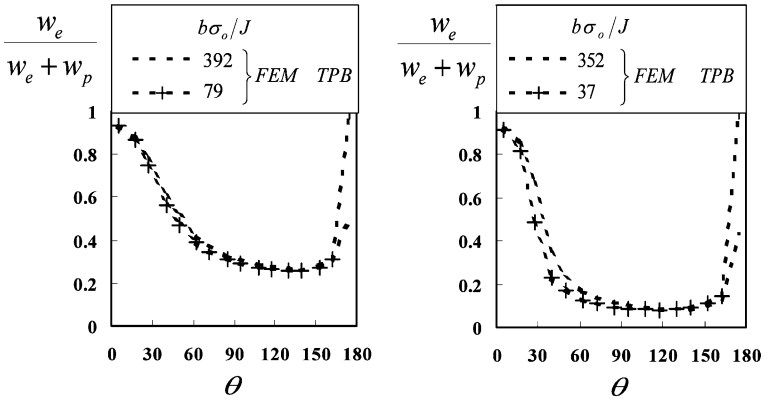

Fig. 14. Angular distribution of the ratio of elastic to total strain energy density.

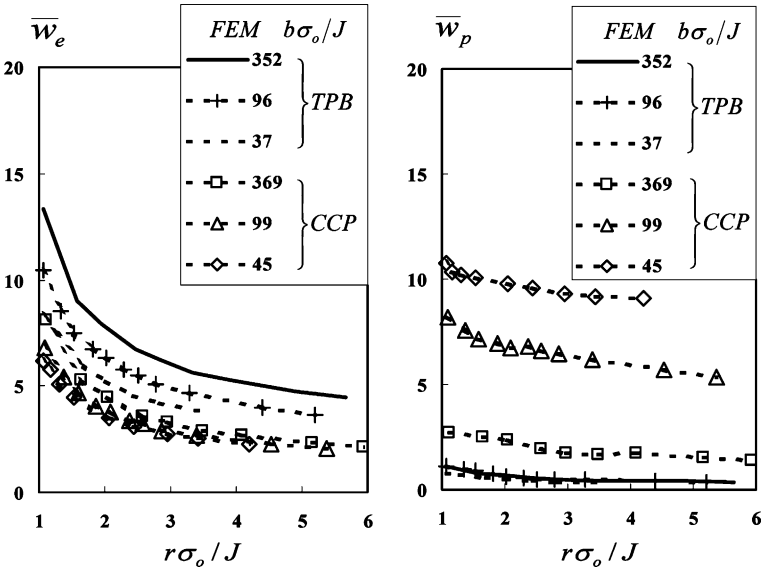

Fig. 15. Ligament distribution of elastic, plastic energy density for $E/E_{\mathrm{p}}=20$.

distributions of the elastic, plastic strain energy densities given by the FEM analyses of $E/E_{\mathrm{p}}=20$ for the two typical specimens are presented in Fig. 15.

As compared with the analytical results presented in Figs. 7 and 9 in Section 4, it is seen that the considerable elastic energy develops on the ligament while little plastic deformation occurs for both the FEM results of TPB specimen and the bi-linear ligament field until T/σ_0 reaches a certain value (about $T/\sigma_0=-1.0$ in Fig. 9). The decrease of the constraint means the decrease of elastic energy density w_{e} and the increase of plastic energy density w_{p} on the ligament.

Again, it is clearly seen that, from high to low constraints, the FEM results of the two typical specimens are similar to the bi-linear ligament field with the T-stress varying from a high to low values (see Figs. 7 and

9). Consequently, the FEM results show that the bi-linear elastic–plastic field with various T-stress values can properly describe different kinds of crack tip fields under various constraints for different specimens.

6. The role of elastic strain energy and fracture criterion

Tian and Wen (2001) reported that the distribution of the energy density is non-uniform in the annulus of $1 < r\sigma_0/J < 6$ around a crack tip. The FEM results presented previously for various crack geometries indicate that the non-uniform distribution of strain energy is a basic feature for all kinds of crack geometries. The high constraint leads to that the high elastic volume energy is accumulated in the forward sector ($0° < \theta < 30°$), while large plastic work occur in the region out of the forward sector. This phenomenon was also found in the HRR field (Tian and Wen, 2001). Therefore, it is true that the plastic dissipation dominates the crack-tip zone when the annulus is considered as a whole. The pattern of the non-uniform distributions of strain energy is dependent on the crack tip constraint, while the constraint is on the specimen geometry, the hardening exponent, and the load level $b\sigma_0/J$. As constrains decreases, the elastic part in the forward sector decreases while the plastic part increases, but in general they are of same order on the ligament.

Yang and Chao (1992) reported that the elastic portion J^e is 12% of the total J in plane strain conditions. Furthermore, the fact that J_c depends on the triaxility of σ_m/σ_e implies that the elastic energy is of importance to the fracture process. The one-parameter fracture criterion of J-integral is based on the HRR field, which was derived from the full plastic model of the deformation theory (or non-linear elasticity by assuming $\sigma_z/(\sigma_r + \sigma_\theta) = 0.5$ and omitting the linear elastic portion). In the HRR field, there is no deformation on the ligament ahead of a crack tip (Tian and Wen, 2001). The one-parameter J-integral criterion is only related to J^p with no relation to the elastic energy. Particularly, it is not related to the deformation induced by hydrostatic stress because of the assumption of $\sigma_z/(\sigma_r + \sigma_\theta) = 0.5$. However, the measured J values from testing specimens include both J^e and J^p. As the above-mentioned, the patterns of the non-uniform energy distributions disappear gradually with the decreasing of the constraint v_{ep}. For high constraint specimens (such as TPB), as the load increases (i.e., as $b\sigma_0/J$ decreases) the ratio of elastic to plastic deformation (i.e. v_{ep}) keeps low steady curves (see Fig. 13(b)). Therefore, the ratio of J^e to J^p keeps high and this leads to low testing values of J_c. By contrast, for low constraint specimens (such as CCP), the curves of v_{ep} is high (see Fig. 13(b)) and the ratio of J^e to J^p decreases. As a result, it leads to the higher testing values of J_c. These phenomena imply that fracture will not occur until the elastic energy is accumulated to a critical value ahead of the crack tip.

By comprising Eqs. (30a), (30b) with (31b), (31c) or Fig. 9 with Fig. 10, the following approximate relations are found,

$$(\bar{w}_{ep})_I \approx \bar{w}_e; \quad (\bar{w}_{ep})_{II} \approx \bar{w}_p. \tag{32}$$

These approximate relations reveal the physical meanings of the above-mentioned two terms. More importantly, if the 'fracture' is assumed to be mainly related to the release of elastic strain energy (since the plastic strain energy dissipated and cannot be released), a fracture criterion can be proposed on the basis of Eq. (31b), that is

$$\left[\frac{(1-2v_{ep})}{(1-v_{ep})}J\right]_C = \text{Const.} \tag{33}$$

Specifically, in linear elastic cases, $v_{ep} = v$ and $J_{Ic} = (1-v^2)K_{Ic}^2/E$, Eq. (33) becomes

$$\left[\frac{(1-2v_{ep})}{(1-v_{ep})}J\right]_C = \frac{(1-2v)}{(1-v)}J_{Ic} = \frac{(1-2v)(1+v)}{E}K_{Ic}^2 = \text{Const.} \tag{34}$$

Since E, v and J_{Ic} are material constants in linear elastic cases, the critical value of J for elastic–plastic problem is determined as,

$$J_c = \left[\frac{(1-v_{ep})}{(1-2v_{ep})}\right]_C \cdot \frac{(1-2v)}{(1-v)} J_{Ic}. \tag{35}$$

For example, in the typical case of $r\sigma_0/J = 1$, combining Eqs. (26b), (27a) and (35) leads to an analytical relation between J_c and T-stress,

$$\left.\begin{aligned} &(1-v_{ep}+v_{ep}^2)\left(\tfrac{T}{\sigma_0}\right)^2 + \left[\frac{(1-2v_{ep})^5}{2\pi(1-v_{ep}^2)(1-2v)\varepsilon_0}\right]^{\frac{1}{2}} \tfrac{T}{\sigma_0} = \left[\frac{(n_p-1)(0.5-v_{ep})}{(n_p-1)(0.5-v_{ep})+v-v_{ep}}\right]^2 - \frac{(1-2v_{ep})^3}{2\pi(1-v_{ep}^2)(1-2v)\varepsilon_0}, \\ &v_{ep} = 1 - \left[2 - \frac{(1-2v)}{(1-v)}\frac{1}{(J_c/J_{Ic})}\right]^{-1}. \end{aligned}\right\} \tag{36a}$$

and this relation can be expressed as

$$J_c/J_{Ic} = f(T/\sigma_0, v, \varepsilon_0, n_p). \tag{36b}$$

For the case with $n_p = E/E_p = 20$, $\varepsilon_0 = 0.0028$ and $v = 0.3$ (similar to the materials of Hancock and Cowling, 1980, see Section 3.2), the relation between J_c and T-stress is plotted in Fig. 16.

From Fig. 16 or Eq. (36), the ratio of J_c for $T = -2.0$ over that for $T = 0$ is given as

$$(J_c)_{T=-2.0}/(J_c)_{T=0} = [(J_c)_{T=-2.0}/J_{Ic}]/[(J_c)_{T=0}/J_{Ic}] = 6.50/1.805 = 3.60. \tag{37}$$

At the same time, the ratio of J_c for CCP over that for TPB is also obtained based on the fracture data of HY80 steel (Hancock and Cowling, 1980),

$$(J_c)_{TPB}/(J_c)_{CCP} = 580.8/190.4 \text{ Mpa} = 3.05. \tag{38}$$

The fact that these two values in Eqs. (37) and (38) are nearly same indicates that the theoretical results is in good agreement with the test results although it is a rough estimation. It is also noted that the FEM results of TPB and CCP are similar to those of the bi-linear field of $T = 0$ and $T/\sigma_0 = -2.0$ respectively as discussed in Section 5.

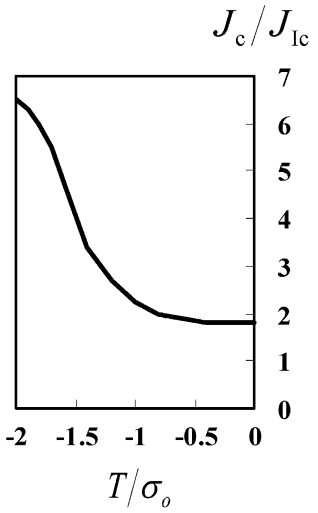

Fig. 16. An analytical curve between J_c and T-stress for $E/E_p = 20$.

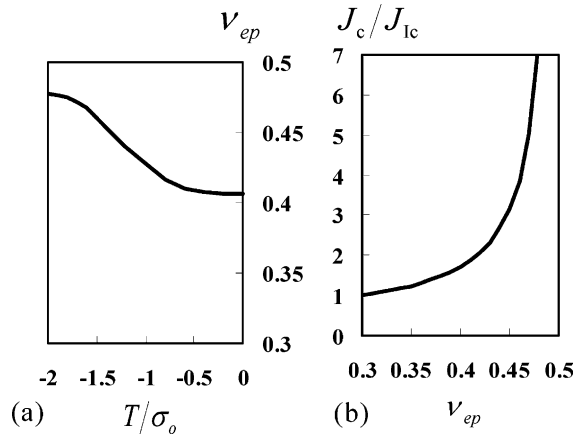

Fig. 17. The analytical curves between v_{ep}, T and J_c, v_{ep} for $E/E_p = 20$. (a) v_{ep}, T relation (b) J_c, v_{ep} relation.

Fig. 16 or Eq. (36) provides a straightforward way to evaluate J_c in term of T-stress for elastic–plastic fracture. This analytical relation is helpful in fracture experiments. Further careful examination of this relation by more experimental data for various materials is expected. It is also noted that T-stress as the second parameter in the linear elastic fracture (Williams, 1957) has been generalized to be used in the elastic–plastic fracture (Betegon and Hancock, 1991). However, this kind of $K - T$ or $J - T$ approach has limited application in the elastic–plastic region because it was based on elasticity theory. In the present study, the relation of J_c and T-stress given by Fig. 16 has no this limitation because it is based on the bi-linear elastic–plastic ligament field.

Meanwhile, Eq. (36a) gives the dependence of v_{ep} on $\overline{T} = T/\sigma_0$, namely,

$$v_{ep} = v_{ep}(T/\sigma_0, v, \varepsilon_0, n_p). \tag{39}$$

The relation between v_{ep} and T-stress for the same materials is shown in Fig. 17(a).

The relation between J_c and v_{ep} given by Eq. (35) is shown in Fig. 17(b) where two extreme cases of most interest are given. The first is the linear elastic case in which $v_{ep} = v$ and $J_c = J_{1c} = (1 - v^2)K_{Ic}^2/E$. In elastic–plastic cases, the J_c depends not only on these two elastic material constants J_{1c}, v, but also the elastic–plastic Poisson's ratio v_{ep} ahead of crack tip. The more the plastic deformation takes place near the crack tip, the larger the factor of $1/(1 - 2v_{ep})$ is, and therefore the larger the value of J_c is. The second extreme case is the full plastic problem in which $\sigma_z/(\sigma_r + \sigma_\theta) = v_{ep} \to 0.5$ and $J_c/J_{Ic} \to \infty$, which implies that the failure criterion may be established by classical strength theory rather than fracture theory.

7. Summary and conclusion remarks

The present analysis is limited to the annulus of $1 < r\sigma_0/J < 6$, in which it is assumed that there is no microcrack phenomenon and no plastic volume deformation. And the J_2-deformation plasticity theory with bi-linear hardening is used to describe the constitutive behaviour of the material.

A Model-I elastic–plastic crack-tip field is obtained by introducing a new constraint variable of v_{ep}, and its physical significance for plane strain elastic–plastic problems is addressed. An analogy scheme for determining the crack-tip fields is proposed. The scheme has been proved to be good approximations although the compatibility equation is not exactly satisfied. We managed to avoid using the separable stress function of the common asymptotic method and to avoid adding the higher-order terms into the solution.

The near-tip elastic–plastic energy distributions are studied with an emphasis on the elasticity in the sensitive region ahead of the crack. Attention is focused on two special cases: one is the first term of $T/\sigma_0 = 0$ for high constraint crack-tip field and the other is the ligament field of different T-stress values for different constrains. It is concluded that the elastic energy cannot be omitted, although the elastic energy is smaller than plastic dissipation when crack tip is taken as a whole.

By comparing the bi-linear fields with the results of detailed finite element analyses, the near-tip stress field as well as the energy field are validated. The FEM analyses indicate that the bi-linear field is physically reasonable and the bi-linear ligament field in terms of T-stress can describe different kinds of crack tip fields under different constraints for different type of specimens. Both the analytical analyses and the FEM results show that the full plastic assumptions of $\bar{\sigma}_e = \sigma_e/\sigma_0 \to \infty$ or $\sigma_z/(\sigma_r + \sigma_\theta) = 0.5$ are not applicable in the region ahead of the crack tip.

An analytical relation between J_c and T-stress for elastic–plastic fracture is established, which is found in good agreement with the test results contributed by Hancock and Cowling (1980). This supports the point that elastic energy in the sensitive region ahead of crack is of importance in fracture process. The analysis of the near-tip strain energy distribution and the constraint condition provides useful insight into the structure of crack-tip fields and is helpful in understanding the ductile fracture process as well as in constructing reasonable failure criteria.

Acknowledgements

The authors are grateful to Prof. S.W. Yu of Tsingua University (China) for helpful suggestions.

References

ANSYS Version 5.6.2, 2000. (ANSYS Inc., Southpointe, 275 Technology Drive, Canonsbury, PA 15317, USA). China Ship Scientific Research Center, Wu'Xi, China.

Begly, J.A., Lands, J.D., 1972. The J-Integral as a fracture criterion in fracture toughness testing. ASTM STP 514, 1–23.

Betegon, C., Hancock, J.W., 1991. Two parameter characterization of elastic–plastic crack tip fields. Journal of Applied Mechanics 58, 104–110.

Chao, Y.J., Yang, S., 1992. Singularities at the apex of a sharp V-notch in a linear strain hardening material. International Journal of Fracture 57, 47–60.

Guo, W.L., 1993. Elastoplastic three dimensional crack border field: Part I—Singular structure of the field. Engineering Fracture Mechanics 46, 93–104.

Hutchinson, J.W., 1968a. Singular behavior at the end of a tensile crack in a hardening material. Journal of the Mechanics and Physics of Solids 16, 13–31.

Hutchinson, J.W., 1968b. Plastic stress and strain field at a crack tip. Journal of the Mechanics and Physics of Solids 16, 337–347.

Hutchinson, J.W., 1983. Fundamentals of the phenomenological theory of nonlinear fracture mechanics. Journal of Applied Mechanics 50, 1042–1051.

Hancock, J.W., Cowling, M.J., 1980. Role of state of stress in crack tip failure process. Metal Science 14, 293–304.

Li, Y.C., Wang, Z.Q., 1986. High-order asymptotic field of tensile plane-strain nonlinear crack problems. Scientia Sinica A 29, 941–955.

McMeeking, R.M., 1977. Finite deformation analysis of crack tip opening in elastic–plastic materials and implications for fracture. Journal of the Mechanics and Physics of Solids 25 (5), 357–381.

McMeeking, R.M., Parks, D.M., 1979. On criteria for J-dominance of crack tip fields in large scale yielding. ASTM STP 668, 175–194.

O'Dowd, N.P., Shih, C.F., 1991a. Family of crack tip fields characterized by a triaxiality parameter: Part I—Structure of fields. Journal of the Mechanics and Physics of Solids 39, 989–1105.

O'Dowd, N.P., Shih, C.F., 1991b. Family of crack tip fields characterized by a triaxiality parameter: Part II—Fracture application. Journal of the Mechanics and Physics of Solids 40, 939–963.

Rice, J.R., Rosengren, G.R., 1968. Plane strain deformation near a crack tip in a power-law hardening material. Journal of the Mechanics and Physics of Solids 16, 1–12.

Rice, J.R., 1974. Limitations to the small scale yielding approximation of elastic–plastic crack-tip fields. Journal of the Mechanics and Physics of Solids 22, 17–26.

Sharma, M.S., Aravas, N., 1991. Determination of higher-order terms in asymptotic elastoplastic crack tip solution. Journal of the Mechanics and Physics of Solids 39, 1043–1072.

Shih, C.F., German, M.D., 1981. Requirement for a one parameter characterization of crack tip fields by HRR singularity. International Journal of Fracture 17 (1), 27–43.

Shih, C.F., 1985. J-dominance under plane strain fully plastic condition: the edge crack panel subject to combined tension and banding. International Journal of Fracture 29, 73–84.

Tian, C.L., Wen, J., 2001. Non-uniform distribution of energy density near a crack tip in the framework of HRR model. International Journal of Fracture 110, L45–50.

Williams, M.L., 1957. On the stress distribution at the base of a stationary crack. Journal of Applied Mechanics 24, 109–114.

Xia, L., Wang, T.C., Shih, C.F., 1993. High-order analysis of crack tip fields in elastic-power hardening materials. Journal of the Mechanics and Physics of Solids 41, 665–689.

Yang, S., Chao, Y.J., 1992. Asymptotic deformation and stress fields at the tip of a sharp notch in an elastic–plastic material. International Journal of Fracture 54, 211–224.

Yang, S., Chao, Y.J., Sutton, M.A., 1993. Higher order asymptotic crack tip fields in a power-law hardening materials. Engineering Fracture Mechanics 45 (1), 1–20.